Multi-User Terahertz WLANs with Angularly Dispersive Links

Keerthi Priya Dasala
Rice University, Houston, Texas, USA
keerthi.dasala@rice.edu

Edward W. Knightly
Rice University, Houston, Texas, USA
knightly@rice.edu

ABSTRACT

THz communication can realize the next order of magnitude in data rate and user densities due to the availability of wide THz-scale spectral bands. Wide bandwidth links can exhibit angular dispersion, i.e., frequency-dependent radiation direction. While angular dispersion has enabled path discovery and dynamic beam steering via frequency tuning, multi-user communication in THz links remains an unaddressed challenge.This paper presents the first study and performance evaluation of multi-user THz WLANs with angularly dispersive links. We employ a single parallel-plate Leaky-Wave Antenna (LWA) for THz directional transmission and present a multi-user communication strategy that exploits angular dispersion and angular separation of users and provides all-spectrum access to users located in different directions with the objective of aggregate rate maximization. With analytical model-driven evaluations and over-the-air experiments, we show how the multi-user performance of an angularly dispersive LWA link fundamentally depends on frequency, angle, and bandwidth utilized by users, through non-linear mechanisms. As increasing bandwidth yields a larger signal footprint in LWA links, we demonstrate that as compared to the model prediction, not only is aggregate data rate maximized with wider beams, but that the experimental link is far better even for practical irregular beams with side lobes and asymmetry. Our experiments demonstrate that by exploiting angular dispersion and users' angular separation, we can transmit without contention or medium access control up to 11 simultaneous users.

CCS CONCEPTS

• **Networks** → **Network protocol design**; *Mobile networks*; *Wireless access networks.*

KEYWORDS

Multi-User WLANs, Terahertz, Beam Steering, Leaky Wave Antenna

ACM Reference Format:
Keerthi Priya Dasala and Edward W. Knightly. 2022. Multi-User Terahertz WLANs with Angularly Dispersive Links . In *The Twenty-third International Symposium on Theory, Algorithmic Foundations, and Protocol Design for Mobile Networks and Mobile Computing (MobiHoc '22), October 17–20, 2022, Seoul, Republic of Korea.* , 10 pages. https://doi.org/10.1145/3492866.3549725

MobiHoc '22, October 17–20, 2022, Seoul, Republic of Korea

ACM ISBN 978-1-4503-9165-8/22/10…$15.00
https://doi.org/10.1145/3492866.3549725

1 INTRODUCTION

Recent advances in WLANs have employed multi-user MIMO to realize multi-Gb/sec data rates via multiplexing multiple data streams in 60 GHz, as standardized in IEEE 802.11ad/ay [10, 19]. Today, THz communications is envisioned as the key building block to realize the next order of magnitude in data rate and user densities for the next generation wireless networks [1, 7, 8, 14], thanks to the availability of the ultra-large bandwidth (0.1 to 1 THz) in THz spectrum. These THz links exhibit a unique property of angular dispersion, where higher frequencies radiate with maximum power towards smaller angles. Yet, due to the high pathloss in THz regime, directional transmission is required and therefore Leaky Wave Antennas (LWA) which work on the same principle of angular dispersion stands to a promising candidate for for THz scale networking. The steering capabilities coupled with the wide bandwidth support offered by angularly dispersive links such as such as those based on LWAs has enabled beam steering by a simple mechanism of tuning the carrier's center frequency [16] and efficient path discovery [11]. While all these works demonstrate the capabilities of angularly dispersive links to transmit and receive directional transmission from a single user, realizing multi-user communication with angularly dispersive THz links is still an open problem.

In this paper, we perform the first performance evaluation of multi-user communication in THz WLANs with angularly dispersive links. In particular, we make the following contributions. First, we characterize the key elements of a wideband multi-user LWA link. We describe how the frequency-angle coupling property manifests via a simplified physics based analytical model. In particular, since LWA is a parallel plate waveguide with an emission slot [22], we treat the LWA slot as a finite length aperture which produces a diffraction pattern in the far field and fit closed form approximations for the single-antenna radiation pattern [12, 24]. We then design the analytical model to characterize the SNR, bandwidth utilization and rate in wideband multi-user LWA link.

The key challenge in multi-user LWA links is determining how the spectral resources can be efficiently allocated to the users to target aggregate rate maximization. To achieve this, we propose All-Spectrum Access with Angular Dispersion (*A3D*), an all-spectrum access transmission scheme that allows different simultaneous users to access the entire spectrum by sharing a single beamformed transmission from the AP, despite being at different locations. The core idea is to exploit the key source of rate gain in SNR diversity among users due to angular dispersion, i.e., inherent differences in the spectral content of users at varying locations to manage the inter-user interference and maximize aggregate rate. To study *A3D* , we define two baselines impacted by angular dispersion: *i)* Frequency Allocation with Angular Dispersion (*FAAD*) that restricts spectral reuse and exploits the users' spectral profiles to optimize the best frequencies split that yields a maximum aggregate rate, and *ii)* Time Allocation with Angular Dispersion (*TAAD*) policy that

allows users to utilize the entire spectrum like *A3D* , however, for a predefined time allocation.

Third, we numerically study the multi-user performance based on the aforementioned physical model. We begin with a simple yet important baseline case of two simultaneous users and characterize the achievable aggregate rate for varying inter-user angular separation. We demonstrate that multi-user aggregate rates vary non-linearly with the location-specific spectral profiles of users owing to the inverse and non-linear nature of the LWA's fundamental coupling between frequency (bandwidth) and angle.

Finally, we perform the first experimental study of multi-user angularly dispersive THz links using over-the-air measurements. By measuring a wideband THz transmission from a custom LWA, we find that the measured spectrum spans lower frequencies and a wide range of emission angles as compared to the model prediction. Despite the beam asymmetry and irregularities in the measured LWA radiation pattern, we demonstrate that the aggregate rates for varying angular separation of users in experimental links is far more better as compared to the model with increasing emission angles. Next, because wider bandwidth corresponds to a wider beamwidth in LWA links, the situation may appear dire that a less directional transmission is assumed to achieve lower aggregate rates. Contrary to our expectation, we show that LWA's beamwidth and bandwidth can simultaneously result in a gradual but increasing aggregate data rate. While wider beams introduce inter-user interference depending on angular separation of users, we show that *A3D* efficiently exploits the varying SINR at the users to achieve closer to 1.5× gains over *FAAD* and *TAAD* systems. Lastly, we explore scaling the number of simultaneous users from 2 to 8. We experimentally show that beamforming to 8 simultaneous users using *A3D* results in 1.5× aggregate rate improvement over *FAAD* and *TAAD* schemes. Indeed, *A3D* heavily relies on angular dispersion and never loses rate even when the group size increase further to 11 users, thus making it a contention-free and scheduler-free transmission policy up to a grouping limit.

2 MULTI-USER LWA LINK FOUNDATIONS

In this section, we describe the main elements of a multi-user wideband LWA THz LoS link, and introduce a simple numerical model characterizing the SNR and achievable data rate over the link. We later describe multiple multi-user transmission strategies that represent how the AP with LWA allocates the spectral resources to users in order to maximize aggregate rate.

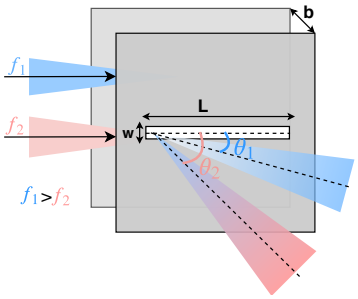

Figure 1: LWA beam steering - the larger the input frequency, the lower the emission angle

2.1 Primer on Angularly Dispersive LWAs

A LWA as shown in Fig. 1 can be realized using a parallel-plate waveguide with an opening in one of the plates to permit radiation to "leak" out into free space. We can treat the leaky waveguide slot as a finite-length aperture, which produces a diffraction pattern in the far-field. For a diffracting aperture (i.e., slot length) of L and the dominant Transverse Electric (TE_1) mode, the far-field radiation radiation pattern G can be derived as [17]:

$$G(f,\theta) \propto sinc\left([\beta(f) - j\alpha + k_0 \cos\theta]\frac{L}{2}\right) \quad (1)$$

where $sinc(x) = \sin x/x$, α is a parameter that describes the loss of energy in the guided mode due to leakage out of the slot, $\beta(f)$ is the frequency-dependent propagation constant of guided waves, k_0 is the free-space wave vector number (i.e., $k_0 = \frac{2\pi f}{c}$) in which c is the speed of light and f is frequency), and θ is the propagation angle of the free-space wave relative to the waveguide's propagation axis ($\theta = 0$ corresponds to emission parallel to the LWA's plates).

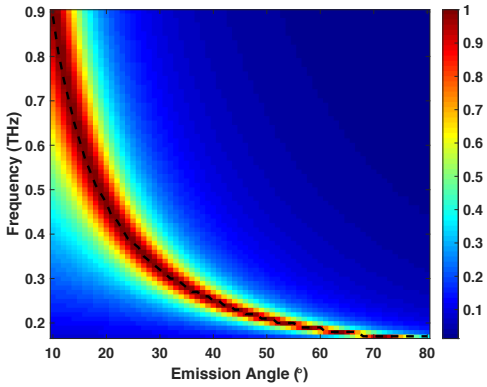

Figure 2: Spectrum-Angle radiation heatmap.

Based on the radiation pattern described in Eq. (1), the energy emitted at a particular angle is coupled with the frequency of the input signal. For a finite slot length, a wide range of frequencies radiate towards a particular emission angle, where the spectral peak is given by

$$f_{max}(\theta) = \frac{c}{2b\sin\theta} \quad (2)$$

where b is the plate separation. Eq. (2) suggests that the larger the input frequency, the lower the max-power emission angle from the slot. This relationship between the angle of emission and frequency makes this device a promising candidate for beam steering at frequencies above 0.1 THz by tuning the input frequency.

While Eq. (2) describes the spectral peak in the direction of a given emission angle, the spectral bandwidth for a receiver in the antenna's far-field can be approximated as [13]:

$$B(\theta) \propto \left|\frac{d}{d\theta}\left(\frac{c}{2b\ \sin\theta}\right)\right| = \left|\frac{c}{2b\ \sin\theta\ \tan\theta}\right| \quad (3)$$

Eq. (3) shows that the antenna's bandwidth (half-power or otherwise) decreases non-linearly with increasing angle, i.e., the LWA can support wider bandwidths for the same beamwidth when transmitting at small emission angles.

Fig. 2 shows an example TE_1 radiation pattern for a LWA with a plate separation of $b = 1\ mm$, slot length $L = 3\ cm$, attenuation constant $\alpha = 200\ rad/m$, and cutoff frequency 150 GHz. The frequency

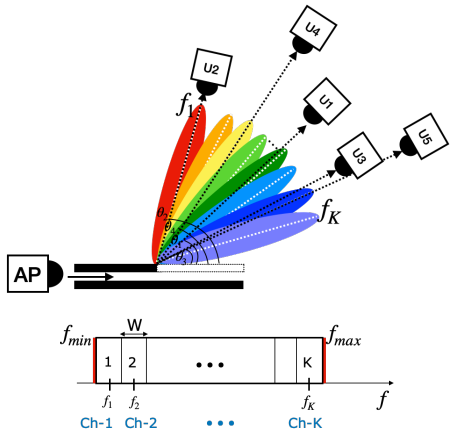

Figure 3: Multi-User LoS link consisting of a LWA, a broadband transceiver at the AP, and broadband receivers at users

range spans from 150 GHz to 900 GHz for a receiver located from 10° to 80°. First, observe the nonlinear frequency angle coupling relationship described by Eq. 2 shown in black dotted lines: lower frequencies emit towards larger angles whereas higher frequencies emit towards smaller angles. Second, the angular spread of each single-tone frequency component determined by attenuation coefficient, α, which controls the increase in peak directivity at a given frequency, and bandwidth at a particular angle.

2.2 Single-User LWA Link Characterization

Consider a static AP with a single LWA sector communicating with multiple users, each equipped with a THz broadband receiver, as shown in Fig. 3. The n^{th} user's, ($\forall$ n $\in \{1, \ldots, N\}$), angular location relative to the AP is given by the emission angle, θ_n. We assume that AP has acquired user's location θ_n via a path discovery phase, and is ideally known (for evaluation). Both the AP and users are assumed to be frequency-agile, having broadband transceivers.

2.2.1 Transmission Bandwidth and Power. A broadband signal, spanning frequencies from $[f_{min}, f_{max}]$ is injected into the transmitter's (AP's) LWA. f_{min} is the minimum operating frequency of the waveguide for the TE_1 guided mode ($= \frac{c}{2b}$), which is 150 GHz, for a plate separation b of 1 mm. Unless stated otherwise, $f_{max} = 1$ THz. The total transmission bandwidth is divided into subchannels of subchannel bandwidth $W = \frac{(f_{max} - f_{min})}{K}$ and centered at f_k for $k \in 1, 2, \cdots, K$. All subchannels have uniform transmit power spectral density, P_t. As illustrated in Fig. 3, the entire space is filled with THz signals such that different frequencies (within the bandwidth of the source) are simultaneously directed to different angles across the entire angular range. The power spectrum of signals leaking from the waveguide can reach users located at a range of angles, albeit encountering different coupling losses. To understand this, we next describe the angle-dependent contributions of the AP's LWA filter to the spectrum of the received signal at the users.

2.2.2 LWA Angle-dependent Spatial Filtering. The LWA imposes a frequency-dependent coupling loss on the radiation emitted in the direction of the user located at θ_n. We denote $D(\theta_n, f)$ as the directivity gain or the coupling loss that a LWA imposes on a given frequency f in the direction of θ_n. This is given as the ratio of the power radiated in a given direction to the average radiated power over all angles in the plane [12]:

$$D(\theta_n, f) = K_0(f) \frac{|G(\theta_n, f)|^2}{\frac{1}{\pi}\int_0^{\pi} |G(\theta_n', f)|^2 d\theta_n'} \tag{4}$$

where $K_0(f)$ is an empirical normalization factor to ensure that the directivity gain for a given frequency f has maximum value of 1 (0 dB), which happens at the peak angle $\theta_{max}(f)$ corresponding to f, from Eq. (2), i.e., $K_0(f) = \frac{1}{D(\theta_{max}(f), f)}$. This results in the power on the k^{th} frequency subchannel, f_k in the signal impinging on the user n LWA being proportional to

$$y_n(f_k) = P_t D(\theta_n, f_k) \left(\frac{c}{4\pi d_n f_k}\right)^2 \tag{5}$$

where d_n is the distance between the AP and user, c is the speed of light and $(\frac{c}{4\pi d_n f_k})^2$ is the free-space path loss between the AP and user n. Thus, we can model the SNR of user n on the frequency subchannel f_k in a LWA link as

$$SNR(\theta_n, f_k) = \frac{P_t D(\theta_n, f_k)(\frac{c}{4\pi d_n f_k})^2}{N_0 W} \tag{6}$$

where the denominator denotes noise power spectral density which is assumed to be flat across the whole transmission band.

2.2.3 Modulation and Coding Scheme (MCS) Limits. While in principle, the user can utilize the entire spectrum from f_{min} to f_{max}, practical receivers have a minimum sensitivity requirement. Therefore, we consider that all available subchannels are used provided the subchannel SNR according to Eq. (6) is above a minimum threshold, SNR_{min}. This can correspond to, for example, a base rate of BPSK rate 1/2 for MCS-0. Given that the SNR will vary significantly depending on the user's location, the total bandwidth that the user utilizes (i.e. number of subchannels with SNR > SNR_{min}) varies significantly with θ_n. We additionally limit the maximum SNR to SNR_{max}, which can correspond to maximum MCS on a given subchannel.

This results in the effective SNR being given by

$$\begin{aligned} SNR_{eff}(\theta_n, f_k) = \min(&SNR(\theta_n, f_k), SNR_{max}) \\ &\times \mathbb{1}\{SNR(\theta_n, f_k) > SNR_{min}\} \end{aligned} \tag{7}$$

where $\mathbb{1}\{SNR(\theta_n, f_k) > SNR_{min}\}$ is an indicator function which equals 1 if the SNR is greater than the minimum threshold and zero otherwise.

2.3 All-Spectrum Access with Angular Dispersion

We present *A3D* , as a spectrum access policy that enables multiple users at different angular locations to share the same time-frequency transmit beam at the AP. This means that all users simultaneously access the spectrum without splitting any degrees of freedom (frequency or time resources) provided by the angularly dispersive LWA links. For example, to serve two users with sufficient angular separation, *A3D* relies on angular dispersion to limit the multi-user interference to enable these angularly separated users to share the same time-frequency beamformed transmission. A single-lobed beam transmission in conventional non-angularly dispersive links would perform poorly with high angular separation due to at least one of the users having low SNR. In contrast,

the LWA link results in frequency-dependent emission in the spatial domain resulting in non-uniformity of received SNRs at users. Thus, *A3D* exploits this diversity of SNRs arising from angularly separated users to manage the inter-user interference and provide high aggregate rate.

To realize *A3D* , we decompose the wideband multi-user LWA link into a set of independent point-to-point channelized links, each having interference as well as thermal noise. Multiple users per sub-channel reduce the signal-to-interference-plus-noise ratio (SINR) of each user's subchannels by an amount that depends on their relative angles.

In particular, *A3D* considers a target set of N backlogged users selected for downlink transmission. Let K denote the number of frequency subchannels within the total transmission bandwidth. Each subchannel frequency $k(1 \leq k \leq K)$ is assigned uniform transmit power spectral density P_t. For user n $(1 \leq n \leq N)$ located at θ_n, we compute the rate per subchannel with center frequency f_k considering that the $SINR(\theta_n, f_k)$ is impacted by the interference from the simultaneous use of the subchannel by other users located at θ_m, $\forall\ m \neq n$, given as

$$R(\theta_n, f_k, W) = \mathrm{W}\log_2\left(1 + \frac{\mathrm{P_t D}(\theta_\mathrm{n}, \mathrm{f_k})\left(\frac{\mathrm{c}}{4\pi \mathrm{d_n f_k}}\right)^2}{\sum_{m\neq n}\mathrm{P_t D}(\theta_\mathrm{m}, \mathrm{f_k})\left(\frac{\mathrm{c}}{4\pi \mathrm{d_m f_k}}\right)^2 + N_o W}\right) \tag{8}$$

The aggregate achievable data rate of user n is the sum of rates across different subchannels as

$$R(\theta_n) = \sum_k R(\theta_n, f_k, W) \tag{9}$$

A key consideration for MU access is determining the number of users to transmit to (group size) and select the members of the group (user selection). In practice, if we have a grouping limit that is beyond the number of backlogged users, then the grouping problem is perhaps trivial, and all the users can spectrum access with angular dispersion. Therefore, *A3D* policy can radically simplify the design and operation with angular dispersion to allow contention-free, scheduling-free access up to to a grouping limit. We experimentally study this problem in Sec. 4.5.

2.4 Frequency Allocation with Angular Dispersion

Here, we present *FAAD* as a baseline spectrum allocation policy that allocates each channel to whichever user has the highest SNR (and thus data rate) for that channel. In particular, *FAAD* specifies the set of frequencies allocated to a target group of users in a multi-user downlink transmission. This policy targets maximizing the aggregate rate of a user group by finding the optimal set of frequencies so that the user with the highest SNR obtains each subchannel. Thus, *FAAD* policy exploits the *a priori* known angular dispersion characteristics of the antenna radiation pattern of the LWA links to allocate the frequencies in a deterministic yet efficient way. Hence, without the angular dispersion, *FAAD* does not exist as all the frequencies are the same and do not have non-uniformity in SNR from the angular dispersion.

Note that, unlike *A3D* , *FAAD* splits the frequencies, and multiple users cannot reuse the same frequency even if there is a benefit of obtaining a better rate found in *A3D* . Thus, *FAAD* systems are ill-suited for universal frequency reuse, implying that *FAAD* incurs a penalty of poor spectral reuse compared to *A3D* .

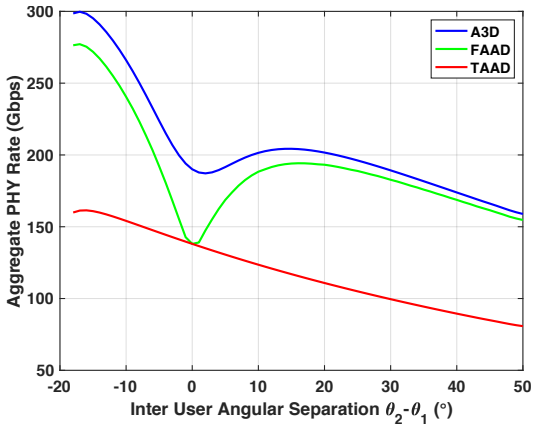

Figure 4: Comparison of aggregate PHY rate of a two-user transmission over a LWA link under *A3D* , *FAAD* , and *TAAD* .

2.5 Time Allocation with Angular Dispersion

In *A3D* , if the multi-user gains start to decline such that one of the users does not achieve minimum rate (MCS-0: BPSK rate 1/2) due to the growing interference of users, then there is no further gain to use *A3D* . This suggests a nearly-optimal multiple access strategy where users have to follow the time alternating all-spectrum access because using *A3D* further would hurt the system's performance. Thus, we introduce *TAAD* as a baseline scheme to *A3D* that targets to maximize the aggregate rate of a grouped set of users by allowing the users to access the entire spectrum in predefined time instances.

Because angularly dispersive links mean that at small emission angles, the user can potentially utilize higher frequencies with larger bandwidths than at large emission angles. Consequently, near-maximum rates are achievable for only a small set of angles, despite the user getting full access to the entire bandwidth. Indeed, one can maximize the aggregate rate by transmitting to a single user located at small emission angles all the time and letting the users at disadvantageous angular locations starve. We can see that this is not a good policy design. Therefore, *TAAD* specifies that each user is allowed full access to the spectrum at different time instances in a way that the time allocated to each user optimally maximizes the rate attainable at each direction. Hence, *TAAD* chooses the time-split as a function of angular dispersion.

3 QUANTIFICATION OF MULTI-USER RATE DEPENDENCY ON INTER-USER ANGULAR LOCATIONS

Since an angularly dispersive link's SNR and data rate is dependent on emission angle, frequency, and bandwidth in a non-linear way, here, we numerically characterize the multi-user performance in wideband LWA links using the numerical model in Sec. 2.

Research Question. For the receiver locating towards small emission angles, higher frequencies spanning a larger bandwidth dominates the spectrum of the signal impinging at the user. In comparison, at larger emission angles, lower frequencies, which

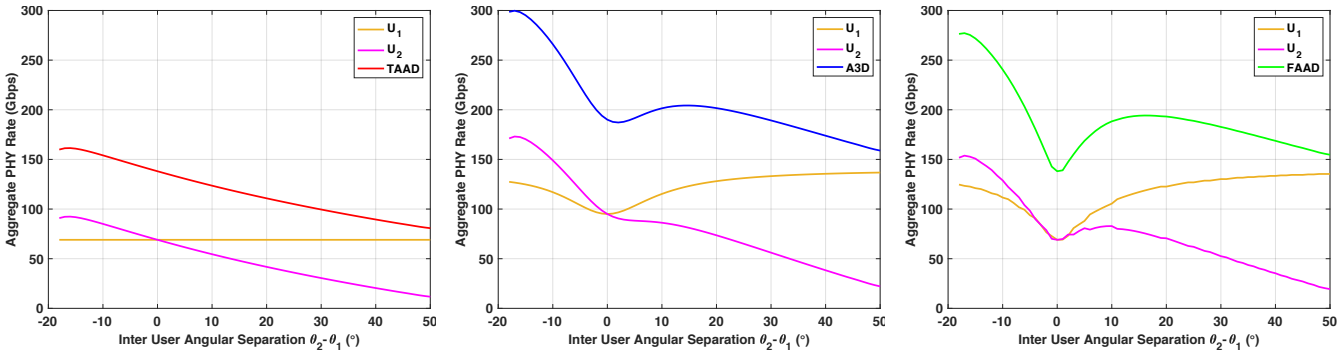

Figure 5: Comparison of aggregate PHY rate obtained by U_1 and U_2 for varying angular separation under (a) *TAAD* , (b) *A3D* , and (c) *FAAD* schemes.

experience smaller path loss (Eq. (6)) spanning a smaller bandwidth, account for most of the power in the impinging signal. The difference in the spectral content of the signal incident at the user's receiver at small versus large angles thus differently impacts link rate in each case. This means that different user locations affect the aggregate rate differently when extended to a multi-user scenario. That is, the difference in the spatial-spectral profiles of the users in one angular regime versus the other would mean sharper the variation in aggregate rate in one angular regime versus the other. To investigate the underlying mechanisms that control this rate behavior, we consider a two-user group for simultaneous transmission and numerically characterize the multi-user performance.

Setup. We consider a fixed AP communicating with two radially aligned users U_1 and U_2, similar to the setup shown in Fig. **??**. We consider U_1 to be always at a fixed angular location θ_1 while U_2's location θ_2 is varied radially around U_1 in steps of 1°. Both the emission angles, θ_1, θ_2, are the line-of-sight angles between the start of the AP's LWA aperture and the broadband transceiver aperture at the users. To demonstrate an example scenario, we assume U_1 locates at 30° and U_2 locates at angles from 12° to 80°. The AP transmits across a total bandwidth $[0.15, 1]$ THz and divides the total bandwidth into subchannels with equal subchannel bandwidth, $W = 3.125$ GHz each with constant transmit power spectral density. In this example, $SINR_{min} = -13$ dB and $SINR_{max} = 15$ dB. Since the SINR on a given subchannel will vary greatly depending on θ_1 and θ_2, the total bandwidth utilized will vary with the locations of these both users. In each setting of $\theta_1 - \theta_2$, we first compute the per user data rate as the the sum of rates across all subchannels as specified under each transmission scheme in Sec. 2. Then, the aggregate PHY rate for each angular separation is given by the sum of data rates obtained by both users across the transmission band. We adopt this computation methodology to record the aggregate rate obtained for all the 3 transmission schemes. The LWA used has same parameters as the example we show in Fig. 2.

Results. Figure 4 shows the aggregate PHY rate of a LWA link supporting two user transmission with varying angular separation under *A3D* , *FAAD* and *TAAD* transmission schemes. We also show the comparison of aggregate rate obtained by each user under each scheme in Fig. 5.

First, observe in Fig. 4 that for an angular separation, $\theta_1 - \theta_2 = -18°$, the aggregate rate obtained by *TAAD* is highest compared to other angular separations in the setup. We can understand this behavior by observing rates of U_1 and U_2 from Fig. 5a. As expected, the signal reaching the user U_2 has much higher bandwidth and thus a higher rate when it locates at a smaller angle (Eq. 3) versus at larger angles, and U_1 achieves a constant rate across all angular separations. However, the decrease in SNR resulting from an increase in emission angle is dominant such that the bandwidth U_2 utilizes decreases, thus contributing to the fall in U_2 data rate and thus aggregate rate as angular separation increases.

Second, although aggregate rates obtained by *A3D* as seen in Fig. 4 is nearly 2× higher than *TAAD* at almost all angular separations in the setup, the performance is not entirely monotonic as as evident from the drop and rise in the magnitude of the aggregate rate as the angular separation varies. Hence, to understand this non-monotonic rate behavior, we divide the locations into three sectors: U_2 smaller than U_1's angle, U_2 closer to U_1 angle, and U_2 larger than U_1's angle. First, when U_2 locates at smaller angles than U_1, its SINR is highly impacted at lower frequencies where U_1 has dominantly higher SNR. As a result, U_2's SINR is highly skewed towards lower frequencies, and thus the higher frequencies and few usable lower frequencies contribute towards the sum rate of U_2, with the net effect of a higher sum rate compared to U_1 as verified from Fig. 5b. Although *FAAD* achieves 1.75× gains over *TAAD* , it has slightly lower aggregate rates than *A3D* . While *FAAD* finds the best set of frequencies based on the maximum achievable SNR at U_2, it allocates only the higher frequencies to U_2 and does not exploit the lower frequencies. Hence the sum rate of U_2 in *FAAD* is lower than that of U_2 in *A3D* . Also, the proportion of frequencies assigned to U_1 vary substantially depending U_2's location, with the sum rate of U_1 more deficient than U_2 at smaller angular separation, as seen in Fig. 5c. A similar argument holds when U_2 moves to large angle sector. The SINR changes at U_2 translates to varying interference at U_1, thereby leading to varying SINR difference at these locations. Thus *A3D* exploits this SINR diversity from the near-far location of users and provides a very reasonable rate to the heavily frequency-biased weak user U_2 while achieving the single-user bound for the strong user U_1.

Interestingly, when the users are co-located with negligible $\theta_1 - \theta_2$, the spectral profiles of users are almost similar. As a result, SINR degrades heavily causing a drop in the multi-user gains achieved by *A3D* as there is no SNR margin to tolerate the interference. Likewise, performance of *FAAD* also drops as *FAAD* optimizes the frequency allocation by dividing the frequencies equally to U_1

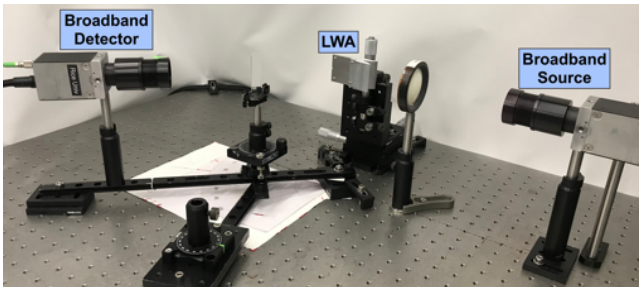

Figure 6: Experimental Setup

and U_2, and as a consequence, degenerates to *TAAD* . Furthermore, observe that *A3D* has sizeable gains over *FAAD* even in this case, as U_2 achieves better rates in *A3D* than *FAAD* at these locations.

Findings: Despite TAAD 's and FAAD 's ability to optimally allocate resources to each user independently, multi-user transmission using A3D exploits the non-uniform and frequency-dependent changes in SINR of users to successfully provide sizeable rate gains over FAAD for smaller to zero angular separation of users, and close to $2\times$ *rate gains over TAAD at almost all inter-user angular separations.*

4 EXPERIMENTAL EVALUATION

In this section, we perform the first experimental study of the performance of multi-user THz LWA link, in terms of aggregate data rate, using over-the-air LWA measurements.

4.1 Experimental Testbed & Over-The-Air Measurements

We measure the radiation pattern of a custom parallel-plate LWA device for experimental validation. Specifically, the LWA consists of two $4x4\ cm^2$ metal plates with thickness of 1 mm. The two metal plates are connected by spacers at the 4 corners, making the plate separation $b = 1\ mm$. Other the geometrical parameters include the slot length $L = 3\ cm$ and a slot width of $1\ mm$.

To measure the radiation pattern of the LWA, we use T-Ray 4000 TD-THz System [6] for generating and receiving THz signals. Fig. 6 demonstrates our experimental setup. This system enables THz wideband measurements by generating a THz-range wideband source at the transmitter and logging timedomain samples at the broadband detector. The generated spectrum from the transmitter spans the range from below 150 GHz to above 1.5 THz. On the receiver side, with the sampling rate of 12.8 THz (1 sample every 78 femtoseconds) and 4096 time-domain samples, we can observe THz-scale frequencies with a frequency resolution of 3.13 GHz.

During the measurement, the transmitter couples the THz pulse and focuses it to the LWA via a lens. Different frequency components then emit from the LWA slot towards different angles. The broadband detector is placed facing the LWA slot at a distance $d = 25.4\ cm$ from the LWA (cm scale due to sub-μW transmit power over the entire band). The detector has a lens with diameter of $4\ cm$. We place the detector at $12^\circ < \theta < 80^\circ$ with 1° resolution in the measurement. We explore this angular range since we observe that below 12° and above 80°, the leaked waves are close to the noise floor, due to a decrease in the efficiency of coupling from the guided wave to free space near the extrema of the angular range. For each measurement, we obtain the frequency spectrum of the time domain received signal using discrete Fourier Transform. As a result, we obtain a LWA dataset containing the frequency spectrum of all measured angles.

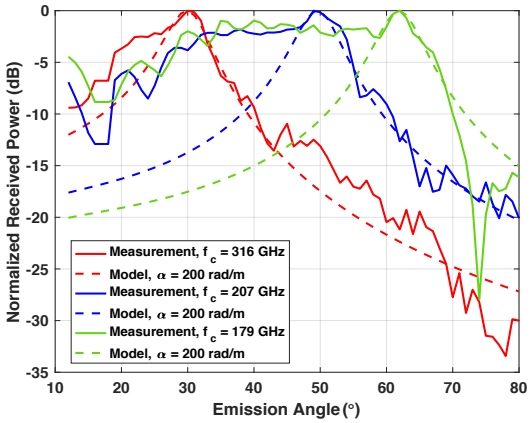

Figure 7: Measured single-tone radiation pattern, matched with model prediction when $\alpha = 200\ rad/m$.

In the following, the same methodology as in the model-driven analysis is used, except that the LWA radiation pattern is based on the over-the-air measurement.

4.2 Comparison between Experimental LWA link and Model Prediction

In order to compare the experimental link with the link based on the numerical model, it is important to first examine the differences and similarities between the two links. This comparison includes the directivity and SNR (Eq. (4)), across different emission angles within a sector and thus higher bandwidths accessible to the user. As discussed in Sec. 3, all of these factors contribute towards the user having access to higher data rates and consequently the attainable aggregate rates in a multi-user scenario.

We experimentally explore the change in the signal amplitude carried by frequency f as we move away from the peak radiation angle, $\theta(f) = \sin^{-1}(\frac{c}{2bf})$. Even though our dataset covers a wide range of frequencies, we include the results for few single tone frequencies, namely, $f = 179, 207$, and $316\ GHz$. To study this, the model parameters are computed from LWA's geometry and we fit the best empirical value of $\alpha = 200\ rad/m$. Fig. 7 shows the measurement results along with the values predicted by model in Eq. 2. We observe that the model predicts the peak angles for all frequencies in our study and has a decreasing trend above and below that peak predicted angle. However, the model underestimates the received power at lower angles. For instance, for $316\ GHz$, the model predicts the peak radiation at 30° but we observe severe discrepancies at lower frequencies where the estimated power is off by 10 dB at some angles. This leads to beam asymmetry in the measurements which is not well captured by the model, also reported in [25]. Moreover, at higher frequencies the measured power decreases with angle with non-monotonic and irregular deviations both above and below the model's prediction. We note that these measurement anomalies are due to the experimental errors.

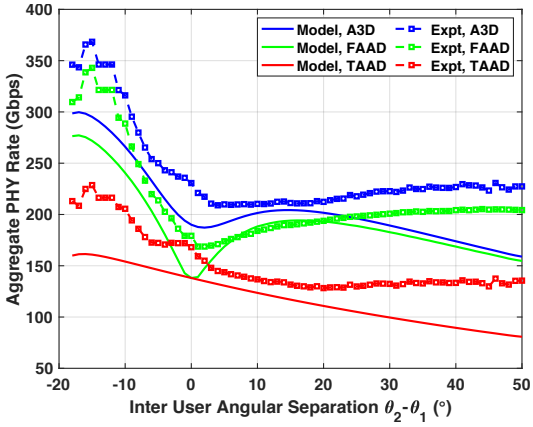

Figure 8: Experimental vs. model aggregate rate of a two-user LWA link under *A3D* , *TAAD* , and *FAAD* schemes.

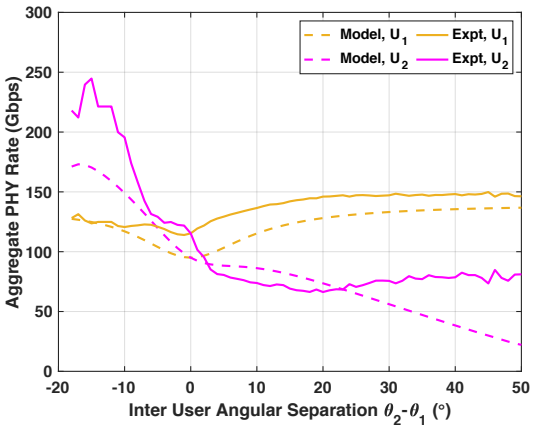

Figure 9: Comparison of experimental vs. model aggregate rate of U_1 and U_2 under *A3D* scheme.

4.3 Multi-User Aggregate Rate and Inter-User Angular Separation

Research Question. As discussed in Section 4.2, there are key differences between the experimental LWA link and model prediction, which can be explained by idealizations in the model that may not be true in practice, such as assuming infinitesimal plate thickness and perfect coupling efficiency. This implies that the beam asymmetry and non-monotonic irregularities in measured beam pattern differently impact the spatial-spectral profiles of the users in one angular regime versus the other and by extension this would mean the sharper variation in experimental aggregate rate of *A3D* in one angular regime versus the other. Hence, we experimentally characterize the multi-user gains of a two-user LWA link.

Setup. We utilize a setup similar to Sec. 3 for computing SNR and utilized bandwidth in the single-antenna link, using the model prediction as a baseline. For the experimental link, the received power spectrum as described in Sec. 4.1 is mapped directly to SNR. For a meaningful comparison, we set $SINR_{max}$= 15 dB and $SINR_{min}$= -12 dB for both the experimental and the model-based link. The transmit power spectral density (PSD) is uniform in the model. The same is not true for the experimental link since we do not have direct access to the non-uniform transmit PSD of the TDS transmitter. Nonetheless, we restrict the bandwidth of operation to within the transmitter's 3-dB bandwidth. In both cases, this results in higher received power at some emission angles as compared to others. Analogous to the process in the numerical analysis in Sec.3, we report the aggregate rate of the two-user LWA link from the measured radiation pattern as a function of inter-user angular separation.

Results. Figure 8 shows the comparison of the experimental and model transmission band aggregate PHY data rate as a function of the inter-user angular separation under *A3D* , *FAAD* , and *TAAD* schemes. The solid lines shows the model predicted aggregate rate based on best matching $\alpha = 200\ rad/m$.

First, we observe that the experimental aggregate rate across all schemes deviates significantly from the model predictions. For example, the experimental aggregate rate of *A3D* at angular separation of -18° is approximately 345 Gbps while the model *A3D* predicts 300 Gbps. These discrepancies have their origins in the LWA radiation pattern prediction errors in Fig. 7. Namely, the peak received power (per frequency) is higher in the experimental link as compared to the model prediction at small emission angles, while the reverse is true at large emission angles. This leads to non-uniform distribution of power across emission angles. Consequently, angular dispersion and beam irregularity result in a non-uniform SNR across the frequency channels for both U_1 and U_2. For example, when the U_2 is located at lower emission angles, it receives stronger signal at higher frequencies compared to the lower frequency channels, whereas U_1 has higher power shifted to lower frequencies with slight power leakage into the high frequencies. Multi-user transmission via *A3D* exploits this resulting SNR diversity arising from the beam asymmetry at varying location of U_2 to its advantage, i.e., the high difference in measurement power between higher and lower frequencies of one user versus the other helps increase the SINR diversity across different angular separation of users. Moreover, the proportion of frequencies with higher SINR at U_1 and U_2, and thus SINR diversity at each angular separation that could result in maximum achievable aggregate rate outweigh those in model prediction, thus leading to a higher aggregate rate in experimental links.

Second, the experimental beams have strong frequency-dependent side-lobes that do not occur uniformly at all angular locations. *A3D* exploits the fact that a strong side-lobe does not happen at the same angle for all frequency channels. That is, while the presence of a strong side-lobe in one frequency channel might translate to higher interference and SINR loss at other user, this is not uniformly evident across all frequencies and all locations. Hence, the effect of side lobes gets averaged out when considering the average of aggregate user rates across the transmission band.

Third, we observe that the experimental aggregate rates is higher than the model aggregate rates with increasing emission angles of U_2 and thus increasing angular separation in the experimental link. Observe from Fig. 8 that the experimental rates for *A3D* above 15° angular separation is not following a decreasing trend like the model and surprisingly, goes up with increasing separation. This is in line with the observation made in Sec. 4.2 that the angular spread of the measured radiation spectrum is considerably greater at all emission angles and is seen to increase with emission angle, and

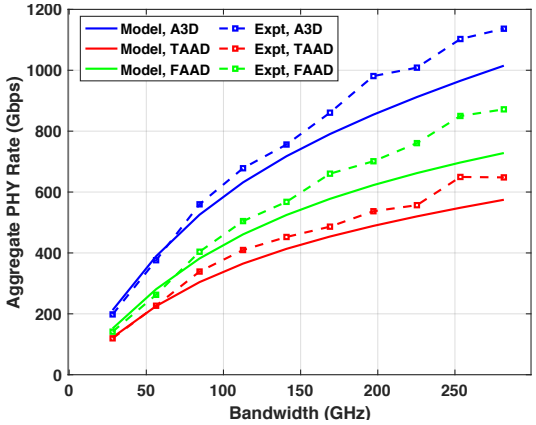

Figure 10: Comparison of experimental vs. model spatial averaged Aggregate PHY rate achieved for varying link bandwidths under *A3D* , *TAAD* , and *FAAD* schemes.

the high directivity power in experimental link is shifted to lower frequencies than model prediction. This observation can be verified from Fig. 9 which shows the users rates achieved in experimental and model links under *A3D* scheme. We can see that the U_1 has a better rate in experimental link than model link across angular separations owing to the high SINR per frequency and thus higher bandwidth at U_1's location. Although U_2 has local fluctuations with model rates, we can see that U_2's rates have the most significant improvements at smaller emission angles, and because of high measurement power at lower frequencies, the rates also improve at higher emission angles. Thus with increasing inter-user angular separation, *A3D* takes advantage of the varying interference diversity leading to better experimental aggregate rates even under asymmetry and irregularities.

Findings. Analysis of the experimental multi-user aggregate rates shows that the measured LWA beams are seen to occupy lower frequencies and smaller emission angles, and has a wider angular coverage with increasing emission angles - hinting that the experimental link has far better aggregate rates than the model prediction even under practical beam irregularities, and the model under-predicting the utilized bandwidth and consequently aggregate data rate at almost all angular separations.

4.4 Bandwidth, Data Rate and Spatial-Signal Footprint

Research Question. For a non angularly dispersive link, the transmission footprint does not change with a larger bandwidth. However, a key property of angularly dispersive links is that the signal footprint widens with a larger transmission band, suggesting a higher data rate and wider angular coverage of users when the bandwidth is larger. Thus far, all policies have had access to all spectrum. Here, we restrict the spectrum in order to examine how widening the bandwidth impacts the performance of different multi-user transmission schemes for the LWA angularly dispersive links.

Setup. We utilize a similar setup as in Sec. 4.3 with the exception that rather than fixing the bandwidth, we consider total transmission bandwidth from 28.2 GHz to 253.3 GHz, indicating low to high bandwidths. In this scenario, U_1 locates at 40° and U_2 location varies from 12° to 80° in steps of 1°. According to the LWA parameters and U_1's location, the center frequency of the transmission is 233.36 GHz. The transmit power is chosen to yield an SNR of 15 dB at U_1 for the center frequency channel. To account for the decrease in directivity as the beam widens with increase in LWA bandwidth we let the normalization factor $K_o(f)$ in the definition of LWA directivity in Eq. 4 be equal to 1. For each value of the transmission bandwidth, we obtain the aggregate PHY rate under each transmission scheme by spatial averaging the aggregate PHY rate achieved for all possible two-user groups.

Results. The results are shown in Fig. 10 which shows the comparison of experimental and model spatially averaged aggregate PHY rate obtained under each transmission scheme.

First, observe that the experimental link exhibits concavity in aggregate rate for increasing bandwidths, with irregular deviations above the model predicted values especially for bandwidths above 50 GHz. For example, at a bandwidth of 112 GHz, *TAAD* achieves approximately 365 Gbps. However, increasing the bandwidth to 225 GHz did not linearly increase the rate. This is because the newly added frequencies have vastly different SNR under the property of angular dispersion. Let us understand counter-intuitive behavior by observing the SNR profile for varying link transmission bandwidths. Recall from Sec. 4.2, that the antenna gain declines slower towards the smaller angle compared to the larger angles. As a result, when the transmission band widens equally from the center frequency, the user located at high emission angle receives a stronger signal for the lower frequency channel than the higher frequency channels, while the trend reverses at smaller emission angles. Thus, we find that user's SNR is more likely to suffer in at least one frequency channel depending on its location. Therefore, the multi-user performance of experimental links is significantly impacted by the asymmetry and irregularities in the radiation pattern and does not scale proportionally with the increasing bandwidth.

Second, from Fig. 10, we find that *FAAD* exhibits similar concavity as *TAAD* but has a better aggregate rate for increasing link bandwidths. Although *TAAD* grants access to the entire spectrum, both the users only get half the air-time, whereas with *FAAD* , the optimal set of subchannel frequencies allocated to the users does not strictly divide in half and exploits the non-uniform yet higher measured SNR at the users, and thus has relatively higher gains than *TAAD* for increasing bandwidths.

Ideally, the *A3D* scheme, would lead to 2× multi-user gains over the *TAAD* scheme. However, it is not the case because, the wider angular spread with increasing bandwidth leads to excessive inter-user interference resulting in reduced SINR at U_2, especially for U_2 positions closer to the U_1. When new frequency channels are added, U_2 receives a similar SNR as U_1 and thus the aggregate rate at this angular separation is only increased by a small constant. The rates only improve for increased inter-user angular separation. That is, when the transmission band widens symmetrically from the center frequency, U_2 has significant SINR only at half of the newly added frequency channels. Meanwhile, U_1 enjoys the rate increment from all the newly added frequency channels. *A3D* naturally takes advantage of the angular-separation varying interference to increase the net aggregate rate as it has the potential to exploit the rate from U_2 as it moves from a high SINR, noise-limited regime to low SINR, interference-limited regime. The SNR loss at U_2 translates to having

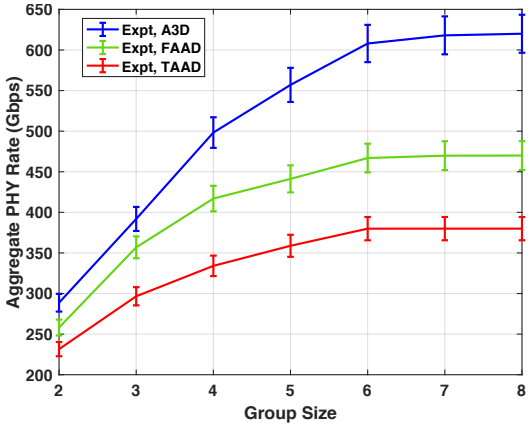

Figure 11: Experimental aggregate PHY rate as a function of the number of users.

lower inter-user interference at U_1, which alone achieves higher than *TAAD* aggregate rate, thus making a higher contribution to the aggregate rate of *A3D* .

Findings. While the experimental aggregate rates increases with increasing bandwidth and better than what the model predicts, the rates scale surprisingly slower owing to the measured beam asymmetry and frequency-dependent side lobes. Nevertheless, A3D can effectively alleviate the disadvantage of inter-user interference from the widening signal footprint and provide relatively consistent and higher aggregate rates over TAAD and FAAD even in practical settings.

4.5 Scaling the Number of Concurrent Users

Thus far, we have considered multi-user transmissions having two users per transmission. Here, we increase group size beyond two to study the viability of further multi-user throughput gains.

Setup. We consider a setup similar to Sec. 4.3 except that we increase the number of users n, from 2 up to 11. The users are uniformly distributed in an angular sector of $[12°, 80°]$. For an n user transmission, we consider all possible user groups consisting of n users out of 69 possible angular locations (i.e., a total of $\binom{69}{n}$ different user groups). Analogous to the process in the experimental analysis in Sec. 4.3, for each group size and each transmission strategy, we first compute the aggregate rate of the n-user LWA link from the measured radiation pattern and then average the performance over all possible user groups.

Results. Figure 11 depicts the achievable experimental aggregate PHY rate as a function of the number of users included in the multi-user transmission under *A3D* , *FAAD* , and *TAAD* schemes.

First, we observe that *A3D* can achieve high experimental aggregate rates, i.e., 392 Gbps and 608 Gbps via simultaneous transmission of three and six users, respectively. The reason for substantial rate increase with group size lies in how *A3D* exploits the multi-user diversity arising from angular dispersion in LWA links. With the increase in group size leading to fluctuations in the SINR of users, the performance of each user depends on the aggregate interference level of the group. For instance, users at smaller emission angles are at high SINR and are noise-limited; the contribution of the interference is relatively small. Users at the larger emission angles, on the other hand, are at low SINR and are interference-limited; the average interference power can be much larger than the background noise. Thus, *A3D* design relies on angular dispersion and fully exploits this SINR diversity provided by averaging the effects of different interfering users in each group. While increasing the number of users in a *A3D* system increases the total level of interference, this allows more graceful degradation of the performance of *A3D* and provides a soft rate limit on the overall multi-user performance.

However, by further increasing the number of users from 6 to 8, the improvement in experimental aggregate rate of *A3D* has diminishing returns and the aggregate rate becomes rate bounded. When seven users are grouped, one user may not contribute enough to the aggregate rate due to excessive user interference. This implies that the multiplexing gain of *A3D* does not endlessly increase with the number of users because the inter-user interference becomes the rate-limiting factor in large group sizes and puts a limit on the number of users admissible under *A3D* . Therefore, the number of simultaneous users that can yield a multi-user gain saturates for a group size of 6 in our setup. Furthermore, we observed in our setup that although *A3D* never loses rate on adding users, the gains start to decline for a group size of 11 users as the high inter-user interference negatively impacts the rate achieved for one of the users to be below the minimum rate (BPSK rate 1/2). Thus, we can use *A3D* without any contention and scheduling control and obtain performance gains by exploiting the angular dispersion to allocate spectral resources with a grouping limit of 11 users.

Second, although *FAAD* achieves 82% of the experimental aggregate rate of *A3D* for a three-user transmission, its performance gap with *A3D* increases with more users. While *FAAD* finds the best set of frequency allocations to users for a group size of 3, unfortunately, its efficiency falls and provides only 70% of the aggregate rate as the group size increases to eight. The reason is, as the number of users sharing the spectrum increases, the proportion of frequencies allocated to users becomes lower, thus making *FAAD* degree-of-freedom limited. Moreover, the users cannot reuse the spectrum, so there is a penalty of poor spectral reuse in *FAAD* compared to *A3D* . Thus the rate contribution of each user towards the sum rate decreases, resulting in saturated gains over *A3D* .

Third, although *TAAD* achieves 74% of the aggregate rate of *A3D* for simultaneous transmission to three users, it has only a marginal aggregate rate increase as the group size increases beyond three. Although *TAAD* allows all users to access the entire spectrum, with each user being added from the growing group size does not contribute enough to the aggregate rate, and with users utilizing equal allocated time ($= \frac{1}{n}$). The orthogonal allocation of time in the *TAAD* system is poorly suited for increasing gains from the viewpoint of interferer diversity and universal spectrum reuse found in *A3D* . Thus implying that *TAAD* evolves to be degree of freedom limited and is overly conservative in admitting users into the network and simultaneously maximizing the aggregate rate gains as group size increases.

Findings. While multi-user beam steering becomes more challenging with increased inter-user interference arising from increasing number of concurrent users, A3D is successfully able to provide 1.3× *and* 1.6× *experimental multi-user rate gains over FAAD and TAAD for simultaneous transmission of* 11 *users.*

5 RELATED WORK

Multi-User Beamforming in Directional Systems. While prior work has not addressed multi-user beamforming at THz, prior work explores spatial multiplexing in mm-Wave spectrum in the context of hybrid analog/digital system architecture design [2, 23], theoretical capacity analysis [20] and user and beam selection algorithms [4, 5]. However, THz spectrum has different propagation characteristics and thus requires different system and node architectures for spatial multiplexing. In contrast to practical antenna arrays in 60 GHz that have wider, irregular beam patterns that do not depend on frequency and result in uniform rate across the transmission band, we study a composite directional THz link with multiple frequency channels which exhibits an angular dispersion property and results in a unique angular spread in space with increasing bandwidth. Moreover, prior work rely on multiple antennas at the transmitter, which cannot be applied to the single antenna system we study. In contrast, this is the first work to perform experimental evaluation of multi-user beamforming for the THz band networks with the single-element LWA link.

Experimental Study of Communication with LWAs. As a key challenge for maintaining directional links, numerous research groups have explored methods for steering THz beams. In the THz range, the parallel-plate LWA has been shown to be a very useful low-loss and low-dispersion platform for many purposes [3, 17, 18, 21]. The steering capabilities coupled with the wide bandwidths offered by angularly dispersive LWA links has led to their application in communication. For example, [13, 16] experimentally demonstrates the capabilities of the LWA to both receive and transmit directional transmissions supporting data rates upto 50 Gb/s. The authors in [15] analyzes interference in a network with LWA transmitters, [25] demonstrated unique security properties of angularly dispersive links, and [9] experimentally shows how the NLoS paths yield higher rate over LoS paths in a single-user LWA link. However, all of these works are focused on LWAs facilitating beam steering towards a single user, this work is the first-ever use of LWA devices to experimentally investigate multi-user THz communication using frequency-dependent beam patterns.

6 CONCLUSIONS

This paper presents the first performance evaluation of multi-user communication in THz WLANs with angularly dispersive links. We proposed *A3D* and using a mix of numerical studies and experimental measurements, we evaluated the multi-user aggregate rate gains as a function of the angular separation of users and showed that exploiting SNR heterogeneity among users is a key source of gain. A unique finding is that the experimental link exhibited far better aggregate rates than the model, even for practical irregular beams with side lobes and asymmetry. We next showed how widening spatial-signal footprint, traditionally a source of rate loss in conventional directional systems, provides a source of multi-user gain for LWA links via *A3D* which exploits the SNR diversity and angular dispersion to limit multi-user interference from widening beams. We further increased group size and demonstrated how our *A3D* scheme stands to be a promising contention-free and scheduler-free candidate scheme for THz-scale networks that supports up to 11 simultaneous users in practice.

7 ACKNOWLEDGEMENTS

This research was supported by Cisco, Intel, NSF grants CNS-1955075, CNS-1923782, CNS-1824529, CNS-2148132 and DOD: Army Research Laboratory grant W911NF-19-2-0269.

REFERENCES

[1] Ian F Akyildiz, Josep Miquel Jornet, and Chong Han. 2014. Terahertz band: Next frontier for wireless communications. *Physical communication* 12 (2014), 16–32.
[2] Ahmed Alkhateeb, Geert Leus, and Robert W. Heath. 2015. Limited feedback hybrid precoding for multi-user millimeter wave systems. *IEEE Trans. on wireless communications* 14, 11 (2015), 6481–6494.
[3] Constantine A. Balanis. 2011. *Modern antenna handbook.* John Wiley & Sons.
[4] Keerthi Priya Dasala, Josep M. Jornet, and Edward W. Knightly. 2020. SIMBA: Single RF Chain Multi-User Beamforming in 60 GHz WLANs. In *IEEE INFOCOM 2020.* 1499–1508.
[5] Keerthi Priya Dasala, Josep M Jornet, and Edward W Knightly. 2021. Uplink Multi-User Beamforming on Single RF Chain mmWave WLANs. In *IEEE INFOCOM 2021.* 1–10.
[6] Irl Duling and David Zimdars. 2009. Revealing hidden defects. *Nature Photonics* 3, 11 (2009), 630–632.
[7] Hadeel Elayan, Osama Amin, Basem Shihada, Raed M Shubair, and Mohamed-Slim Alouini. 2019. Terahertz band: The last piece of RF spectrum puzzle for communication systems. *IEEE Open Journal of the Comms. Society* 1 (2019), 1–32.
[8] John Federici and Lothar Moeller. 2010. Review of terahertz and subterahertz wireless communications. *Journal of Applied Physics* 107, 11 (2010), 6.
[9] Yasaman Ghasempour, Yasith Amarasinghe, Chia-Yi Yeh, Edward Knightly, and Daniel M Mittleman. 2021. Line-of-sight and non-line-of-sight links for dispersive terahertz wireless networks. *APL Photonics* 6, 4 (2021), 041304.
[10] Yasaman Ghasempour, Claudio RCM da Silva, Carlos Cordeiro, and Edward W Knightly. 2017. IEEE 802.11 ay: Next-generation 60 GHz communication for 100 Gb/s Wi-Fi. *IEEE Comms. Magazine* 55, 12 (2017), 186–192.
[11] Yasaman Ghasempour, Chia-Yi Yeh, Rabi Shrestha, Daniel Mittleman, and Edward Knightly. 2020. Single Shot Single Antenna Path Discovery in THz Networks. In *ACM MobiCom '20.*
[12] David R Jackson, Arthur A Oliner, and C Balanis. 2008. Modern antenna handbook. In *Fundamental Parameters and Definitions for Antennas.* Wiley, 1–54.
[13] Nicholas J. Karl, Robert W. McKinney, Yasuaki Monnai, Rajind Mendis, and Daniel M. Mittleman. 2015. Frequency-division multiplexing in the terahertz range using a leaky-wave antenna. *Nature Photonics* 9, 11 (2015), 717–720.
[14] Thomas Kürner and Sebastian Priebe. 2014. Towards THz communications-status in research, standardization and regulation. *Journal of Infrared, Millimeter, and Terahertz Waves* 35, 1 (2014), 53–62.
[15] Zheng Lin, Lifeng Wang, Bo Tan, and X. Li. 2021. Spatial-spectral Terahertz Networks. *ArXiv* abs/2101.02868 (2021).
[16] Jianjun Ma, Nicholas J. Karl, Sara Bretin, Guillaume Ducournau, and Daniel M. Mittleman. 2017. Frequency-division multiplexer and demultiplexer for terahertz wireless links. *Nature communications* 8, 1 (2017), 1–8. Nature Publishing Group.
[17] Rajind Mendis and Daniel Grischkowsky. 2001. Undistorted guided-wave propagation of subpicosecond terahertz pulses. *Optics letters* 26, 11 (2001), 846–848.
[18] Rajind Mendis and Daniel M. Mittleman. 2010. A 2-D Artificial Dielectric With $0 \leq n < 1$ for the Terahertz Region. *IEEE Trans. on Microwave Theory and Techniques* 58, 7 (2010), 1993–1998.
[19] Thomas Nitsche, Carlos Cordeiro, Adriana B Flores, Edward W Knightly, Eldad Perahia, and Joerg C Widmer. 2014. IEEE 802.11 ad: directional 60 GHz communication for multi-Gigabit-per-second Wi-Fi. *IEEE Comms. Magazine* 52, 12 (2014).
[20] Akbar M Sayeed and Vasanthan Raghavan. 2007. Maximizing MIMO capacity in sparse multipath with reconfigurable antenna arrays. *IEEE Journal of Selected Topics in Signal Processing* 1, 1 (2007), 156–166.
[21] Kaushik Sengupta and Ali Hajimiri. 2012. A 0.28 THz power-generation and beam-steering array in CMOS based on distributed active radiators. *IEEE Journal of Solid-State Circuits* 47, 12 (2012), 3013–3031.
[22] Kaushik Sengupta, Tadao Nagatsuma, and Daniel M Mittleman. 2018. Terahertz integrated electronic and hybrid electronic–photonic systems. *Nature Electronics* 1, 12 (2018), 622–635.
[23] Richard A. Stirling-Gallacher and Md Saifur Rahman. 2015. Multi-user MIMO strategies for a millimeter wave communication system using hybrid beamforming. In *IEEE ICC 2015.* 2437–2443.
[24] Adrian Sutinjo, Michal Okoniewski, and Ronald H Johnston. 2008. Radiation from fast and slow traveling waves. *IEEE Antennas and Propagation Magazine* 50, 4 (2008), 175–181.
[25] Chia-Yi Yeh, Yasaman Ghasempour, Rabi Shrestha, Daniel Mittleman, and Edward Knightly. 2020. Security in Terahertz WLANs with Leaky Wave Antennas. In *ACM WiSec '20.*